Quantitative 3D Assessment of ^{68}Ga-DOTATOC PET/MRI with Diffusion-Weighted Imaging to Assess Imaging Markers for Gastroenteropancreatic Neuroendocrine Tumors: Preliminary Results

Lisa C. Adams*[1], Keno K. Bressem*[1], Julia Brangsch[1], Carolin Reimann[1], Kristin Nowak[1], Winfried Brenner[2], and Marcus R. Makowski[1]

[1]*Department of Radiology Charité, Berlin, Germany; and* [2]*Department of Nuclear Medicine, Charité, Berlin, Germany*

^{68}Ga-DOTATOC PET/MRI combines the advantages of PET in the acquisition of metabolic–functional information with the high soft-tissue contrast of MRI. SUVs in tumors have been suggested to be a measure of somatostatin receptor expression. A challenge with receptor ligands is that the distribution volume is confined to tissues with tracer uptake, potentially limiting SUV quantification. In this study, various functional 3-dimensional SUV apparent diffusion coefficient (ADC) parameters and arterial tumor enhancement were tested for ability to characterize gastroenteropancreatic (GEP) neuroendocrine tumors (NETs). **Methods:** For this single-center, cross-sectional study, 22 patients with 24 histologically confirmed GEP NET lesions (15 men and 7 women; median age, 61 y; range, 43–81 y) who underwent hybrid ^{68}Ga-DOTA PET/MRI at 3 T between January 2017 and July 2019 met the eligibility criteria. SUV, tumor-to-background ratio, total functional tumor volume, and mean and minimum ADC were measured on the basis of volumes of interest and examined with receiver-operating-characteristic analysis to determine cutoffs for differentiation between low- and intermediate-grade GEP NETs. The Spearman rank correlation coefficient was used to assess correlations between functional imaging parameters. **Results:** The ratio of PET-derived SUV_{mean} and diffusion-weighted imaging–derived minimum ADC was introduced as a combined variable to predict tumor grade, outperforming single predictors. On the basis of a threshold ratio of 0.03, tumors could be classified as grade 2 with a sensitivity of 86% and a specificity of 100%. SUV and functional ADCs, as well as arterial contrast enhancement parameters, showed nonsignificant and mostly negligible correlations. **Conclusion:** Because receptor density and tumor cellularity appear to be independent, potentially complementary phenomena, the combined ratio of PET/MRI and SUV_{mean}/ADC_{min} may be used as a novel biomarker allowing differentiation between grade 1 and grade 2 GEP NETs.

Key Words: gastroenteropancreatic neuroendocrine tumors; ^{68}Ga-DOTATOC PET/MRI; diffusion-weighted imaging; combined PET/MRI ratio; tumor grades

J Nucl Med 2020; 61:1021–1027
DOI: 10.2967/jnumed.119.234062

Gastroenteropancreatic (GEP) neuroendocrine tumors (NETs) are a rare and heterogeneous group of tumors originating from neuroendocrine cells of the gastrointestinal tract, with a wide spectrum of clinical behavior (*1*).

According to the World Health Organization classification, NETs are divided into grade 1 (≤2% Ki-67 index), grade 2 (3%–20% Ki-67 index), and grade 3 tumors (>20% Ki-67 index), depending on their proliferative activity (*2*). The 5-y survival rates for grade 1 tumors are estimated to be 89%, compared with 70% for grade 2 tumors and less than 57% for grade 3 (*3*), making tumor grading a valuable tool for prognostic assessment. Noninvasive tumor grading in particular would be of clinical benefit, as it could reduce risks associated with biopsy and improve preoperative assessment.

Overexpression of somatostatin receptors in most GEP NETs creates a highly specific target for molecular imaging with ^{68}Ga-labeled somatostatin analogs (e.g., ^{68}Ga-DOTATATE and DOTATOC) and enables the development of new therapeutic approaches (*4*). The introduction of hybrid PET/MRI allowed for simultaneous multiparametric imaging, combining superior soft-tissue contrast and high spatial resolution with functional imaging, such as diffusion-weighted imaging (DWI) or tumor contrast agent enhancement, with the possibility of assessing the intensity or density of somatostatin receptor expression using the SUV (*5,6*). A correlation between somatostatin receptor expression and SUVs was proposed in previous research, supporting a qualification of ^{68}Ga-labeled somatostatin analogs in the diagnostics of GEP NETs (*7*). In addition, PET/MRI with ^{68}Ga-labeled somatostatin analogs also showed potential for the prediction of survival and treatment response in NETs (*8*). However, a challenge with receptor ligands is that the distribution volume is confined to tissues with tracer uptake, potentially affecting SUV quantification.

DWI is an MR-based imaging technique allowing quantification of the degree of water motion by calculation of the apparent diffusion coefficient (ADC). It is recognized as a functional sequence, reflecting

Received Jul. 21, 2019; revision accepted Nov. 13, 2019.
For correspondence or reprints contact: Lisa C. Adams, Department of Radiology and Nuclear Medicine, Charité, Charitéplatz 1, 10117 Berlin, Germany.
E-mail: lisa.adams@charite.de
*Contributed equally to this work.
Published online Dec. 20, 2019.

tumor cell density, but low–b-value images also enable an accurate depiction of anatomy (*9,10*). Previous studies found associations between the ADC and histopathologic tumor features, reporting relationships with proliferation activity in several cancer types and thus showing a potential for predicting the grade of differentiation and prognosis (*11–13*).

To identify the most suitable metric for image-based characterization of GEP NETs, the present study investigated different receptor density–related and functional parameters. Although SUV and ADC measurements, as well as tumor enhancement, are already established in cancer imaging, it is still not clear to what extent they can provide complementary information in the context of tumor differentiation and physiology and whether there is a correlation between such PET and MRI parameters.

The present study therefore had 2 aims. The first was to compare 3-dimensional (3D) SUV and ADC parameters such as SUV_{mean}, SUV_{max}, tumor-to-background ratio (TBR), ADC_{mean} and ADC_{min} (determining the mean and minimum value of all voxels), total functional tumor volume (TFTV), and arterial tumor enhancement across different GEP NET grades, evaluating if they could identify the grade of differentiation with reliable diagnostic accuracy. The second aim was to examine a potential association among 3D SUV, ADVs, and arterial tumor enhancement to determine whether they correlate or are independent.

MATERIALS AND METHODS

Patient Population

Within this cross-sectional study, we prospectively acquired and analyzed 98 ^{68}Ga-DOTATOC PET/MRI examinations performed at our department for diagnostic evaluation of GEP NET between January 2017 and July 2019 (Fig. 1). The study was approved by the Institutional Review Board (EA1/060/16), and before the examinations all subjects gave written informed consent.

Of this consecutive cohort, 22 patients (7 women, 15 men; median, 61 y; age range, 43–81 y) with 24 primary or recurrent NETs met the eligibility criteria (patient older than 18 y, gadolinium-enhanced ^{68}Ga-DOTATOC PET/MRI as the index test, presence of a NET lesion in the gastrointestinal tract as defined by ^{68}Ga-DOTATOC tracer uptake or contrast enhancement, no ongoing systemic therapy). One patient with a grade 3 GEP NET of the pancreas was excluded from analysis due to $n = 1$ not being representative. Table 1 provides an overview of patient and tumor characteristics.

In all patients, the diagnosis of NET was histologically confirmed; histopathologic results therefore served as the reference standard for this study. GEP NETs were classified into 3 grades according to the World Health Organization system by integrating the Ki-67 labeling index and the presence of necrosis. The Ki-67 labeling index was available for all but 1 patient.

Hybrid PET/MRI Imaging Protocol

Simultaneous PET/MRI was performed with a 3-T Magnetom Biograph mMR hybrid MRI/PET system (Siemens Healthcare; software, vB20P), featuring avalanche photodiode and total imaging matrix coil technology. The MR parameters were as follows: gradient: 45 mT/m maximum gradient amplitude; 200 T/m/s maximum gradient slew rate; lutetium oxyorthosilicate crystal; 4.3-mm transverse spatial resolution at full width at half maximum at 1 cm; 15.0 kcps/MBq sensitivity at center; and 13.8 kcps/MBq at 10 cm off-center.

The PET scan started 60 min after injection of ^{68}Ga-DOTATOC (mean activity, 160 MBq), comprising a whole-body scan with 5 bed positions (each being 3 min long [30% overlap]) from the skull base to the upper thigh, with subsequent iterative high-definition PET image reconstruction (3 iterations) based on an x-matrix acquisition with a 4-mm gaussian filter and relative scatter scaling. No adverse effects were observed after the injection of ^{68}Ga-DOTATOC. The unenhanced MRI sequences were acquired simultaneously with a dedicated mMR head-and-neck coil and phased-array mMR body surface coils.

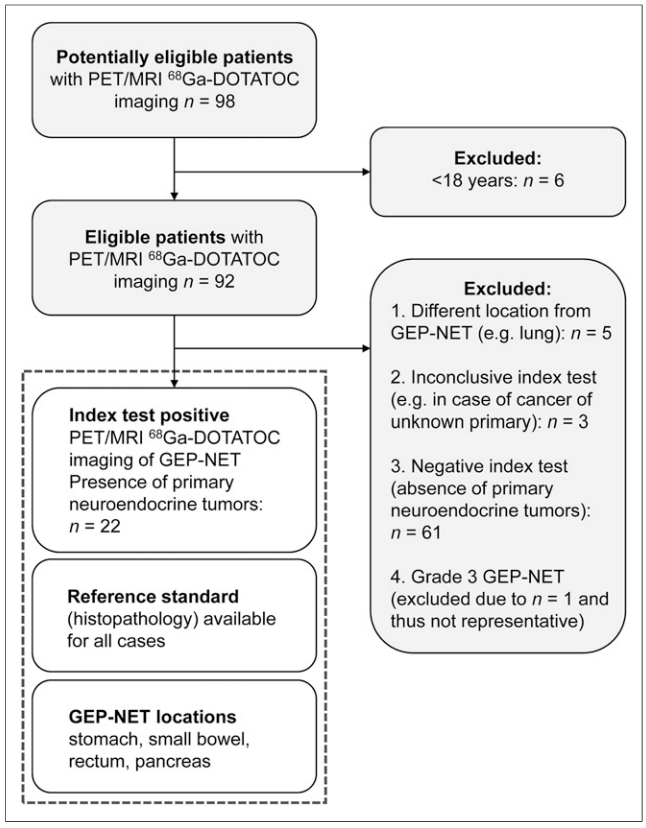

FIGURE 1. Study flowchart.

Table 2 provides an overview of the MRI sequence and tabulated parameters. Gadolinium-based contrast medium was administered at a dose of 0.1 mL/kg of body weight. The delay, as obtained by bolus tracking, was approximately 18 s for the arterial bolus.

The total imaging time for the PET/MR study, including contrast-enhanced MRI, was 90 min. Postacquisition data analysis was performed with syngo.MR General Engine (Siemens Healthcare).

Hybrid PET/MRI Volumetric Imaging Analysis

All imaging datasets were evaluated on a PACS workstation using Visage (version 7.1; Visage Imaging). One experienced radiologist analyzed fused gadobutrol-enhanced ^{68}Ga-DOTATOC PET/MR images and native ^{68}Ga-DOTATOC PET/DWI MR images, identifying NET-positive lesions. On ^{68}Ga-enhanced PET/MR images, focal ^{68}Ga accumulations with any kind of morphologic correlate in a contrast-enhanced or DWI series were regarded as NET-positive. Any discrepancies were resolved through a separate consensus reading. The radiologists were masked to the patient's identity and to the results of previous or follow-up imaging, as well as to histopathology results and tumor grade. To avoid recognition bias, contrast-enhanced ^{68}Ga-DOTATOC PET/MR images and native ^{68}Ga-DOTATOC PET/DWI MR images were assessed in different sessions and random order, separated by 2 wk.

For segmentation, PET/MR images were exported from the PACS as DICOM data and segmented with MITK (*14*). To analyze the functional

TABLE 1
Patient- and Tumor-Related Characteristics

Characteristic	Data
Age (y)	61 (43–81)
Sex	
Male	15 (68.2%)
Female	7 (31.8%)
Histologic tumor grade (24 lesions)	
Grade 1	12 (50%)
Grade 2	12 (50%)
Tumor location	
Stomach	1 (4.2%)
Small bowel	9 (37.5%)
Rectum	1 (4.2%)
Pancreas	13 (54.2%)
Presence of metastases	20 (80.0%)

Qualitative data are expressed as numbers followed by percentages in parentheses; continuous data are expressed as mean ± SD followed by range in parentheses.

volume, a semiautomatically delineated 3D volume of interest (VOI) was obtained in the respective lesion on the PET images, with an isocontour set to 70% of maximum uptake.

Quantitative analysis of ADC parameters was based on the high–b-value images, on which the NETs were best visualized, incorporating voxels across multiple slices. The VOIs were then copied to the ADC maps. Accordingly, the quantitative values within the measured VOI were ADC_{mean} and ADC_{min}. The TFTV was based on an isocontour of 70%, and SUV_{mean} and SUV_{max} were measured within the corresponding 3D VOI. The normalized quantitative TBR was based on the background signal of the healthy tissue adjacent to the lesion.

Lesion or parenchyma contrast-to-noise ratios (CNRs) were defined as the signal intensity of the lesion (SI lesion) minus SI parenchyma divided by the SD of the background noise. The enhancement ratio of the respective lesion before and after the administration of gadolinium was based on the following formula:

$$\text{Enhancement ratio} = (\text{contrast-enhanced SI lesion} - \text{native SI lesion})/\text{native SI lesion}.$$

Statistical Analysis

All statistical analysis was performed using the R statistical environment (version 3.4.4). Values were expressed as mean and SD if normally distributed and as median and interquartile range if not. For most nonnormally distributed lesions, normalization could be achieved through logarithmic transformation. To assess the direction and strength of correlation between 2 variables, Spearman correlation coefficients were calculated. Interpretation was as follows: a positive or a negative correlation coefficient of 0.90–1.00 was considered very high; 0.70–0.89 was considered high; 0.40–0.69, moderate; 0.30–0.49, low; and 0–0.29, negligible (*15*). Box plots were used to display the value distribution among different tumor grades. A receiver-operating-characteristic analysis was then performed to establish a cutoff for differentiation between grade 1 and grad 2 tumors. Significance levels are indicated as $P < 0.05$, $P < 0.01$, $P < 0.001$, and $P < 0.0001$.

RESULTS

There were 12 grade 1 tumors (48.0%) and 12 grade 2 tumors (48.0%). The mean maximum diameter as measured on axial MRI was 29.6 ± 23.8 mm (range, 11–95 mm), and the mean TFTV was 36.8 ± 82.0 cm^3 (range, 1.1–351.1 cm^3) (Table 1).

Comparison of Histologic Grades with Tumor Size, Enhancement, SUV and ADC Parameters, and Tumor Volume (Preliminary Data)

Grade 2 tumors were significantly larger than grade 1 tumors (40.7 ± 30.4 mm [range, 11.0–40.0 mm] vs. 19.7 ± 9.6 mm [range, 12.0–95.0 mm], $P < 0.05$). The TFTV was higher in grade 2 tumors than in grade 1 tumors (70.6 ± 112.2 cm^3 [range, 1.5–351.1 cm^3] vs. 6.4 ± 9.9 cm^3 [range, 1.2–34.2 cm^3], $P = 0.06$)). Among SUV parameters, SUV_{mean} (measured within a 3D VOI) was significantly higher in grade 2 tumors than in grade 1 tumors (23.1 ± 12.3 [range, 8.0–45.0] vs. 14.7 ± 7.0 [range, 4.0–23.2], $P < 0.05$). SUV_{max} was also higher in grade 2 tumors than in grade 1 tumors (42.3 ± 26.6 [range, 14.8–89.5] vs. 34.9 ± 16.9 [range, 14.5–62.5]; however, this

TABLE 2
MRI Sequence Parameters

Sequence	Orientation	Bandwidth (Hz/Px)	TR/TE (ms)	Matrix	FOV (mm)	Voxel size (mm^3)	TA (s)
T2-weighted HASTE	Axial	710	1,400/95	320	400	1.3 × 1.3 × 5.0	68
T2-weighted TIRM	Coronal	300	4,390/53	256	450	1.8 × 1.8 × 4.0	142
T1-weighted fs VIBE	Axial	450	3.9/1.86	320	400	1.3 × 1.3 × 3.0	17
T2-weighted fs TSE	Axial	243	2,200/100	448	400	0.9 × 0.9 × 5.0	230
EPI DWI	Axial	2,232	5,600/55	134	380	1.4 × 1.4 × 5.0	204
T1-weighted fs VIBE (dynamic)	Axial	450	3.95/1.92	320	360	1.1 × 1.1 × 3.0	17 (per phase)
T1-weighted fs STARVIBE (Siemens)	Axial	870	3.05/1.44	320	380	12.x1.2 × 1.2	278

TR = repetition time; TE = echo time; FOV = field of view; TA = time of acquisition; HASTE = half-Fourier acquisition single-shot turbo spin echo; TIRM = turbo inversion recovery magnitude; fs = fat saturation; VIBE = volumetric interpolated breath-hold sequence; EPI = echo planar imaging.

TABLE 3
Comparison of Imaging Parameters Between Different World Health Organization Grade GEP NETs

Parameter	Grade 1 (n = 12)	Grade 2 (n = 12)
Diameter (mm)	19.7 ± 9.6 (12.0–95.0)	40.7 ± 30.4 (11.0–40.0)
TFTV (cm^3)	6.4 ± 9.9 (1.2–34.2)	70.6 ± 112.2 (1.5–351.1)
Ki-67 proliferation index (%)	1.6 ± 0.6 (0.9–2.0)	5.3 ± 2.6 (2.3–10)
TBR	6.6 ± 1.9 (3.1–10.1)	12.7 ± 9.3 (3.9–33.2)
SUV_{mean}	14.7 ± 7.0 (4.0–23.2)	23.1 ± 12.3 (8.0–45.0)
SUV_{max}	34.9 ± 16.9 (14.5–62.5)	42.3 ± 26.6 (14.8–89.5)
ADC_{mean} ($\times 10^{-3}$ mm^2/s)	1.24 ± 0.18 (1.05–1.49)	0.96 ± 0.26 (0.50–1.22)
ADC_{min} ($\times 10^{-3}$ mm^2/s)	0.67 ± 0.14 (0.51–0.87)	0.49 ± 0.24 (0.23–0.85)
Enhancement ratio	1.2 ± 0.8 (0.6–2.9)	1.0 ± 0.4 (0.4 to 1.6)

Data are mean ± SD followed by range in parentheses.

difference was not significant, at $P = 0.25$). Normalized TBRs were also higher in grade 2 tumors than in grade 1 lesions (12.7 ± 9.3 [range, 3.9–33.2] vs. 6.6 ± 1.9 [range, 3.1–10.1], $P < 0.05$). Regarding the ADC parameters measured, grade 2 tumors showed a significantly lower ADC_{mean} than grade 1 tumors (960.7 ± 262.2 [range, 500–1,221] vs. 1,235.9 ± 183.0 [range, 1,045–1,486], $P < 0.05$). ADC_{min} was also lower in grade 2 tumors than in grade 1 tumors; however, these differences were not significant (492.9 ± 244.0 [range, 225.5–849.5] vs. 665.2 ± 135.5 [range, 510.5–868.5], $P = 0.17$). Regarding the evaluation of arterial contrast enhancement, enhancement ratios were marginally higher for grade 1 GEP NETs than for grade 2 GEP NETs (1.2 ± 0.8 [range, 0.6–2.9] vs. 1.0 ± 0.4 [range, 0.4–1.6], $P = 0.5$). 1 shows the lesion characteristics.

Comparing Ki-67 Labeling Index with Tumor Size, Tumor Volume, and SUV and ADC Parameters (Preliminary Data)

The correlation between quantitative 3D imaging parameters and Ki-67 labeling index was analyzed for 22 patients (not available for 1 patient). TFTV showed a positive correlation with Ki-67 ($r = 0.65$, $P < 0.05$), whereas ADC_{mean} showed a weaker correlation ($r = -0.37$, $P = 0.07$). Otherwise, none of the imaging values measured within 3D VOIs correlated at least moderately with Ki-67. Figures 2 and 3 and Supplemental Figures 1 and 2 show examples of 1 grade 1 and 3 different-sized grade 2 GEP NETs (supplemental materials are available at http://jnm.snmjournals.org).

Logistic Regression and Receiver-Operating-Characteristic Analysis

To identify cutoffs for SUV_{mean}, SUV_{max}, TBR, TFTV, and ADC_{mean} and ADC_{min} to differentiate grade 1 from grade 2 tumors, receiver-operating-characteristic analyses were performed. Sensitivity and specificity (1 − false-positive rate) were calculated with varying cutoffs for all variables. The optimal cutoffs were based on the maximum sum of sensitivity and specificity. For SUV_{mean}, the cutoff was 28, which means that 2 tumors could be identified with a sensitivity of 44% and a specificity of 100%

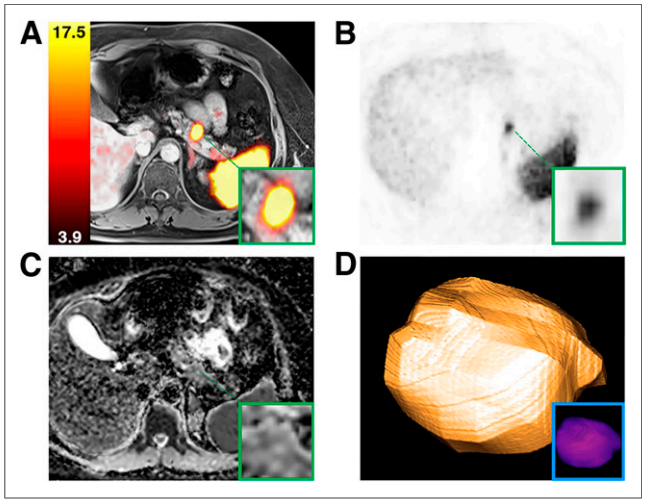

FIGURE 2. Example of 3D VOI lesion analysis in 50-y-old patient with grade 1 pancreas NET (SUV_{mean} of 15 and ADC_{min} of 900 mm^2/s; combined SUV_{mean}/ADC_{min} ratio, 0.02). Shown are fusion of enhanced T1-weighted VIBE (volumetric interpolated breath-hold sequence) MRI with ^{68}Ga-DOTATOC PET (A), ^{68}Ga-DOTATOC PET (B), ADC map (C), and 3D lesion model (D).

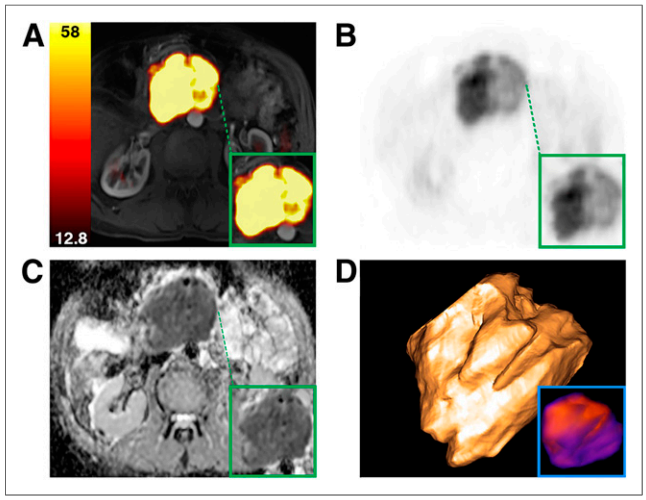

FIGURE 3. Example of 3D VOI lesion analysis in 64-y-old patient with grade 2 pancreas NET (SUV_{mean} of 45 and ADC_{min} of 490 mm^2/s; combined SUV_{mean}/ADC_{min} ratio, 0.09). Shown are fusion of enhanced T1-weighted VIBE (volumetric interpolated breath-hold sequence) MRI with ^{68}Ga-DOTATOC PET (A), ^{68}Ga-DOTATOC PET (B), ADC map (C), and 3D lesion model (D).

if the SUV_{mean} exceeded the cutoff. For SUV_{max}, the cutoff was 67, which means that 2 tumors could be identified with a sensitivity of 22% and a specificity of 100% if the SUV_{mean} exceeded the cutoff. For TBR, the cutoff for 2 tumors to be exceeded was 12, yielding a sensitivity of 56% and a specificity of 100%, and for TFTV, the cutoff to be exceeded was 15.5, resulting in a sensitivity and specificity of 67% and 90%, respectively, For ADC_{mean}, the receiver-operating-characteristic analysis suggested a cutoff of 1.06×10^{-3} mm^2/s, whereby tumors with values less than the cutoff would be graded as 2 (sensitivity, 67%; specificity, 86%). For ADC_{min}, the receiver-operating-characteristic analysis suggested a cutoff of 0.50×10^{-3} mm^2/s, whereby tumors with values less than the cutoff would be graded as 2 with a sensitivity of 67% and a specificity of 100%. For differentiation between grade 1 and grade 2 tumors, SUV_{mean} was superior to SUV_{max}, and ADC_{min} was superior to ADC_{mean}. However, as none of the single predictors provided optimal diagnostic accuracy, the ratio of SUV_{mean} and ADC_{min} was introduced as a combined variable to predict tumor grade, outperforming the single predictors for discrimination between grade 1 and grade 2 tumors. For a threshold ratio of 0.03, tumors could be classified as grade 2 with a sensitivity of 86% and a specificity of 100% (Fig. 4 shows the receiver-operating-characteristic analyses). Figures 2 and 3 show examples of patients with low- and intermediate-grade GEP NETs).

Preliminary Results on the Association Between 3D SUV and ADC and Arterial Enhancement

SUV and ADC showed nonsignificant and negligible correlations (ADC_{min} and SUV_{max}, $r = 0.26$, $P = 0.39$; ADC_{mean} and SUV_{mean}, $r = 0.01$, $P = 0.98$; ADC_{min} and SUV_{mean}, $r = 0.15$, $P = 0.62$; ADC_{mean} and SUV_{max}, $r = -0.05$, $P = 0.88$), suggesting that the SUV- and ADC-based values were independent, as would also be expected from a functional point of view.

Regarding a potential correlation between SUV and contrast enhancement parameters, SUV_{max} and enhancement ratio or SUV_{max} and contrast-to-noise-ratio$_{art}$ (CNR_{art}) showed moderate correlations ($r = 0.67$ or $r = 0.53$, respectively) that did not reach significance levels ($P = 0.13$ or $P = 0.06$, respectively). All other correlations were not significant and were negligible (SUV_{mean} and CNR_{art}, $r = 0.44$, $P = 0.14$; SUV_{mean} and enhancement ratio, $r = 0.2$, $P = 0.52$). Supplemental Figure 3 shows scatterplots of the examined correlations between the SUV and ADC parameters and between the SUV and MRI enhancement values.

DISCUSSION

PET imaging plays a pivotal role in the diagnosis of GEP NETs. Our results suggest that a combined assessment of the complementary parameters 3D SUV_{mean} and ADC_{min} allows for a reliable differentiation between low- and intermediate-grade GEP NETs. Although 3D SUV_{mean} was significantly higher, ADC_{min} was significantly lower in grade 2 tumors than in grade 1 tumors. As is to be expected, considering the underlying functional mechanisms, the present study showed nonsignificant and mostly negligible correlations between ADC and SUV parameters and between ADC and contrast enhancement parameters.

SUV is the most studied semiquantitative parameter in the analysis of tracer uptake in PET imaging and has been suggested as a marker for the quantification of somatostatin receptor density in NETs (*7,16*). Although, so far, data on PET somatostatin receptor studies are limited, some studies suggested that changes in tumor SUV did not reliably correlate with treatment outcome and the net uptake rate (K_i) (*17,18*). Accordingly, SUV may not offer a perfect reflection of somatostatin receptor expression.

Despite the apparent difficulty of establishing a link between tracer avidity and histopathologic tumor grade, it was previously demonstrated that well-differentiated NETs (grade 1 and 2 tumors) showed higher SUVs for ^{68}Ga-labeled somatostatin analogs than did poorly differentiated NETs (*19*). We found a significant difference between low- and intermediate-grade GEP NETs, with intermediate-grade GEP NETs showing a higher ^{68}Ga-DOTATOC uptake, unlike the previously published literature (*19*). We also found SUV_{mean} to be a more reliable predictor than SUV_{max}. But

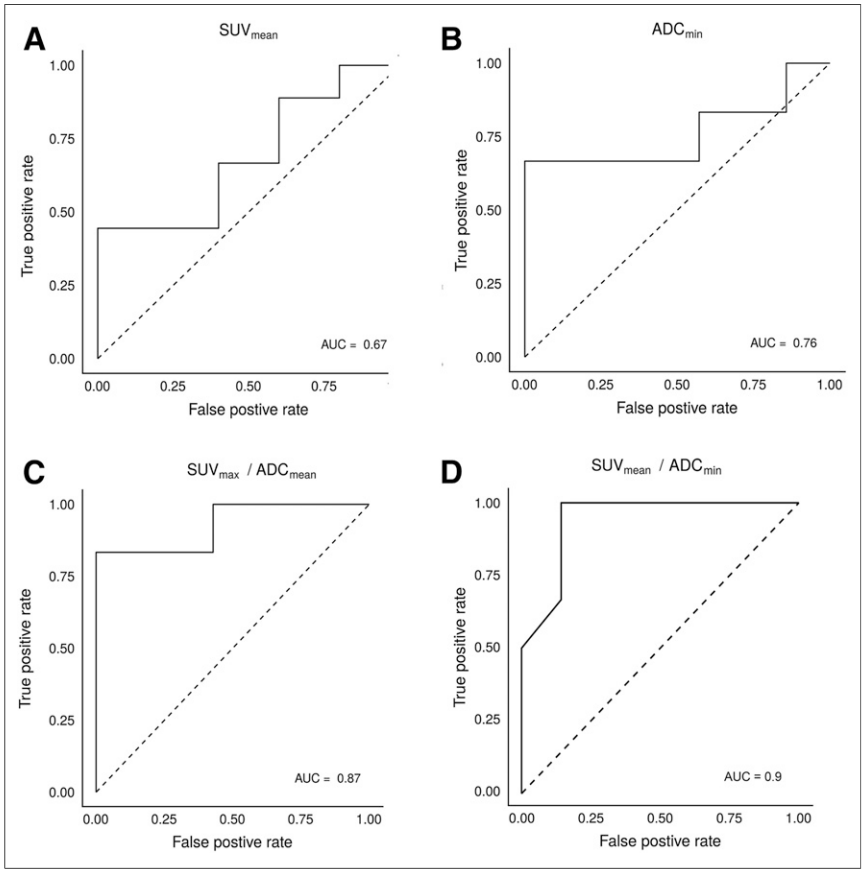

FIGURE 4. Receiver-operating-characteristic curves from ^{68}Ga-DOTATOC PET and MRI ADC parameters. SUV_{mean} demonstrates poor to moderate discriminative test performance (A), whereas ADC_{min} shows fair discriminative ability (B). Of combined ratios and parameters, SUV_{mean}/ADC_{min} (D) demonstrates better discriminative test performance than SUV_{max}/ADC_{mean} (C), with AUC of 0.90, sensitivity of 86%, and specificity of 100%. AUC = area under the curve.

even when using SUV_{mean} as a single predictor for histopathologic grade, only a poor to moderate diagnostic accuracy could be achieved, suggesting that SUV alone cannot be used to assess tumor grade.

Therefore, a complementary approach including SUV_{mean} and ADC_{min} was applied. DWI ADCs are based on a measure of cellularity. Since tumor cellularity is contributed largely by cellular proliferation, the ADC can be considered a surrogate biomarker for tumor-cell proliferation. It may be assumed that malignancies with a high proliferative index have higher cellularity and more restricted diffusion, resulting in lower ADCs. Previously, DWI ADCs demonstrated a potential to distinguish grade 1 from grades 2 and 3 neuroendocrine lesions and also correlated with the Ki-67 index (*20,21*). In line with this finding, we also identified ADC parameters, especially ADC_{min}, as potential predictors to differentiate between grade 1 and grade 2 GEP NETs. Avoiding possible gadolinium-associated risks and as an alternative when contrast agents are contraindicated, DWI could furthermore represent a cost-effective alternative to contrast-enhanced MRI for fused ^{68}Ga-DOTA PET/MRI.

Regarding a potential relationship between SUV and ADC parameters, no correlation could be found, as was to be expected from a functional point of view, considering that ^{68}Ga-DOTATOC–based SUV is a measure of receptor expression and density whereas ADC is a surrogate marker of cellularity and restricted water diffusion. This result is also line with previous research in which ADC and SUVs showed no correlations, irrespective of the underlying histologic subtype, supporting their independence (*16,22*). It can be assumed that SUV and ADC illuminate different aspects of pathophysiology. A combination of PET-based receptor imaging with functional MRI information therefore provides complementary information on tumor characterization. We incorporated 3D SUV and ADC parameters into a single prediction model, which enabled a reliable differentiation between low- and intermediate-grade GEP NET.

Since NETs and their metastases are typically hypervascular, they often show arterial hyperperfusion (*23*). In the present study, we found large variations in this characteristic, particularly because of the heterogeneous, larger tumors, involving nonenhancing cystic, necrotic, or hemorrhagic areas as well as hyperenhancing regions. In line with our findings, Jeon et al. reported hyperenhancement to be present in approximately only half of patients, with iso- or hypoenhancement otherwise present on arterial-phase images (*24*). Regarding a potential association between functional ^{68}Ga-DOTATOC PET/DWI SUV_{max} and arterial enhancement pattern as measured by semiquantitative CNRs, we could identify only a moderate, nonsignificant correlation between SUV_{max} and the enhancement ratio or CNR_{art}.

There are limitations to the present study. Factors that could potentially influence the generalizability of the results include the hardware characteristics (i.e., different PET/MRI systems), the chosen imaging parameters, and the applied delineation technique. A main limitation is the small patient cohort, especially regarding intestinal NET lesions, which may have resulted in type 2 errors. On the other hand, GEP NET is a relatively rare entity and PET/MRI is a novel technique. As there was only 1 case of grade 3 GEP NET, this case was excluded and our analysis was limited to grades 1 and 2 GEP NETs. In addition, regarding the calculation of separate detection rates for contrast-enhanced MRI, DWI/MRI, and PET/MRI, there is an obvious selection bias. Finally, the premise that PET/MRI-based assessment of GEP NETs shows the potential to reduce or even alleviate the need for biopsy in the future might be premature. Further validation with larger patient populations will be required, specifically including grade 3.

CONCLUSION

As receptor expression and tumor cellularity appear to be independent phenomena, the combined PET/MRI ratio SUV_{mean}/ADC_{min}, which is based on 3D measurements of all voxels within the respective lesion volumes, may be used as a novel biomarker to differentiate between grade 1 and grade 2 GEP NETs. Therefore, multiparametric analysis from hybrid PET and DWI might offer the potential to noninvasively acquire complementary, image-based information on the proliferative activity of GEP NETs.

DISCLOSURE

Marcus Makowski receives support from the Deutsche Forschungsgemeinschaft (DFG, SFB 1340/1 2018, 5943/31/41/91). Lisa Adams participates in the BIH Charité–Clinician Scientist Program, which is funded by the Charité–Universitaetsmedizin Berlin and the Berlin Institute of Health. No other potential conflict of interest relevant to this article was reported.

KEY POINTS

QUESTION: Can the combined PET/MRI ratio SUV_{mean}/ADC_{min} serve as a biomarker for differentiation between low- and intermediate-grade primary or recurrent GEP NET, and is there a potential association between functional 3D SUV and ADV, as well as arterial tumor enhancement?

PERTINENT FINDINGS: Receptor density and tumor cellularity appeared to be independent, potentially complementary phenomena.

IMPLICATIONS FOR PATIENT CARE: The combined PET/MRI ratio SUV_{mean}/ADC_{min} may be used as a biomarker to differentiate between low- and intermediate-grade GEP NETs. Multiparametric analysis from hybrid PET and DWI might offer the potential to noninvasively acquire complementary, image-based information on the proliferative activity of GEP NETs, providing incremental diagnostic value beyond anatomic imaging.

REFERENCES

1. Díez M, Teule A, Salazar R. Gastroenteropancreatic neuroendocrine tumors: diagnosis and treatment. *Ann Gastroenterol.* 2013;26:29–36.
2. Saeger W, Schnabel PA, Komminoth P. Grading of neuroendocrine tumors [in German]. *Pathologe.* 2016;37:304–313.
3. Richards-Taylor S, Ewings SM, Jaynes E, et al. The assessment of Ki-67 as a prognostic marker in neuroendocrine tumours: a systematic review and meta-analysis. *J Clin Pathol.* 2016;69:612–618.
4. Haug AR, Cindea-Drimus R, Auernhammer CJ, et al. The role of ^{68}Ga-DOTATATE PET/CT in suspected neuroendocrine tumors. *J Nucl Med.* 2012;53:1686–1692.
5. Paidpally V, Chirindel A, Lam S, Agrawal N, Quon H, Subramaniam RM. FDG-PET/CT imaging biomarkers in head and neck squamous cell carcinoma. *Imaging Med.* 2012;4:633–647.
6. Koukouraki S, Strauss LG, Georgoulias V, et al. Evaluation of the pharmacokinetics of ^{68}Ga-DOTATOC in patients with metastatic neuroendocrine tumours scheduled for ^{90}Y-DOTATOC therapy. *Eur J Nucl Med Mol Imaging.* 2006; 33:460–466.
7. Kaemmerer D, Peter L, Lupp A, et al. Molecular imaging with ^{68}Ga-SSTR PET/CT and correlation to immunohistochemistry of somatostatin receptors in neuroendocrine tumours. *Eur J Nucl Med Mol Imaging.* 2011;38:1659–1668.
8. Kaewput C, Suppiah S, Vinjamuri S. Correlation between standardized uptake value of ^{68}Ga-DOTANOC positron emission tomography/computed tomography

and pathological classification of neuroendocrine tumors. *World J Nucl Med.* 2018;17:34–40.
9. Taouli B, Koh DM. Diffusion-weighted MR imaging of the liver. *Radiology.* 2010;254:47–66.
10. Zech CJ, Herrmann KA, Dietrich O, Horger W, Reiser MF, Schoenberg SO. Black-blood diffusion-weighted EPI acquisition of the liver with parallel imaging: comparison with a standard T2-weighted sequence for detection of focal liver lesions. *Invest Radiol.* 2008;43:261–266.
11. Surov A, Meyer HJ, Wienke A. Associations between apparent diffusion coefficient (ADC) and KI 67 in different tumors: a meta-analysis. Part 2: ADCmin. *Oncotarget.* 2018;9:8675–8680.
12. Sasaki T, Kim J, Moritani T, et al. Roles of the apparent diffusion coefficient and tumor volume in predicting tumor grade in patients with choroid plexus tumors. *Neuroradiology.* 2018;60:479–486.
13. Higano S, Yun X, Kumabe T, et al. Malignant astrocytic tumors: clinical importance of apparent diffusion coefficient in prediction of grade and prognosis. *Radiology.* 2006;241:839–846.
14. Wolf I, Vetter M, Wegner I, et al. The medical imaging interaction toolkit. *Med Image Anal.* 2005;9:594–604.
15. Mukaka MM. Statistics corner: a guide to appropriate use of correlation coefficient in medical research. *Malawi Med J.* 2012;24:69–71.
16. Fruehwald-Pallamar J, Czerny C, Mayerhoefer ME, et al. Functional imaging in head and neck squamous cell carcinoma: correlation of PET/CT and diffusion-weighted imaging at 3 Tesla. *Eur J Nucl Med Mol Imaging.* 2011;38:1009–1019.
17. Velikyan I, Sundin A, Sorensen J, et al. Quantitative and qualitative intrapatient comparison of ^{68}Ga-DOTATOC and ^{68}Ga-DOTATATE: net uptake rate for accurate quantification. *J Nucl Med.* 2014;55:204–210.
18. Kratochwil C, Stefanova M, Mavriopoulou E, et al. SUV of [^{68}Ga]DOTATOC-PET/CT predicts response probability of PRRT in neuroendocrine tumors. *Mol Imaging Biol.* 2015;17:313–318.
19. Kayani I, Bomanji JB, Groves A, et al. Functional imaging of neuroendocrine tumors with combined PET/CT using ^{68}Ga-DOTATATE (DOTA-DPhe1,Tyr3-octreotate) and ^{18}F-FDG. *Cancer.* 2008;112:2447–2455.
20. Jang KM, Kim SH, Lee SJ, Choi D. The value of gadoxetic acid-enhanced and diffusion-weighted MRI for prediction of grading of pancreatic neuroendocrine tumors. *Acta Radiol.* 2014;55:140–148.
21. Wang Y, Chen ZE, Yaghmai V, et al. Diffusion-weighted MR imaging in pancreatic endocrine tumors correlated with histopathologic characteristics. *J Magn Reson Imaging.* 2011;33:1071–1079.
22. Goense L, Heethuis SE, van Rossum PSN, et al. Correlation between functional imaging markers derived from diffusion-weighted MRI and ^{18}F-FDG PET/CT in esophageal cancer. *Nucl Med Commun.* 2018;39:60–67.
23. Worhunsky DJ, Krampitz GW, Poullos PD, et al. Pancreatic neuroendocrine tumours: hypoenhancement on arterial phase computed tomography predicts biological aggressiveness. *HPB (Oxford).* 2014;16:304–311.
24. Jeon SK, Lee JM, Joo I, et al. Nonhypervascular pancreatic neuroendocrine tumors: differential diagnosis from pancreatic ductal adenocarcinomas at MR imaging-retrospective cross-sectional study. *Radiology.* 2017;284:77–87.